

Effect of Anodization Parameters on the Surface Morphology and Photoelectrochemical Properties of TiO₂ Nanotubes

Shenghan Zhang*, Yanqing Li, Peiyao Xu, Kexin Liang

Department of Environmental Science and Engineering, North China Electric Power University, No. 689, Huadian Rd. Baoding City, Hebei, P.R.China.

*E-mail: zhang-shenghan@163.com

Received: 28 July 2017 / Accepted: 19 September 2017 / Published: 12 October 2017

Titanium sheets are anodized to prepare titanium dioxide nanotubes (TiO₂ NTs) with varying chemical polishing times, anodizing voltages, anodizing times and NH₄F electrolyte concentrations. The surface morphology of the TiO₂ NTs is observed by a Scanning Electron Microscope (SEM) and used to characterize the inner diameter (d_i), centre to centre distance (l) and wall thickness (w). The photoelectrochemical performance of TiO₂ NT arrays is described by measurements of the photocurrent density and the incident photon to current efficiency (IPCE). The data show l can be controlled by the anodizing voltage; in contrast, d_i and w are influenced by the anodizing time and NH₄F electrolyte concentration. Furthermore, the effects of the anodization parameters on the TiO₂ NTs' surface morphology were determined to influence each other. Using the optimum condition of an anodizing voltage of 60 V at 60 min in 0.125 mass % NH₄F ethylene glycol, TiO₂ NTs were fabricated that showed a photocurrent density of 90.42 $\mu\text{A}/\text{cm}^2$ and maximum IPCE of 18.76 % at 300 nm. The results indicate that the effects of the anodization parameters on the photocurrent response of TiO₂ NTs are primarily achieved through control of the wall thickness and the ratio of the diameter to the wall thickness (d_i/w). For a wall thickness that is greater than a critical value, the ratio d_i/w can reach a range in which the TiO₂ NTs show a high photocurrent output.

Keywords: TiO₂ nanotubes; anodization; surface morphology; photoelectrochemical property; wall thickness

1. INTRODUCTION

Nano titanium dioxide (TiO₂) is a versatile inorganic material with a wide range of applications, such as dye-sensitized solar cells [1, 2], photocatalysis [3], sensors [4, 5] and bio-medical coatings [6]. In the past two decades, self-organized TiO₂ nanotubes (NTs), fabricated by electrochemical anodization of Ti, have been widely investigated due to their flexibility, simplicity of formation, highly ordered structure and directional pathways for electron transport [7]. TiO₂ NTs with

varying morphological characteristics and photoelectrochemical performance can be obtained by anodization under different conditions [7-10]. Formation of well-defined nanotube structures depends on a number of anodization parameters, such as the applied voltage, temperature of the electrolyte, concentration of fluoride, and anodizing time [8, 10-12]. Recent reports have discussed the mechanisms for the formation of TiO₂ NTs based on field-assisted dissolution theory (FAD) [13], flow model [14], avalanche breakdown theory [15] and oxygen bubble mold (OBM) [16].

In contrast, previous studies have also investigated the impact of various factors on the photoelectrochemical properties of TiO₂ NTs for a more quantitative examination of the influence of the morphology of the NTs [17-19]. However, systematic data are still lacking [20-22].

In this paper, we examined the surface morphology and photoelectrochemical properties of TiO₂ NTs grown using different anodizing voltages, anodizing times and NH₄F electrolyte concentrations. The relationship between the anodization parameters and properties of the TiO₂ NTs was demonstrated. Moreover, the fabrication of TiO₂ NTs was optimized using a combination of three kind of anodization parameters to realize good photoelectrochemical properties with good reproducibility.

2. EXPERIMENTAL

2.1. Sample pretreatment

Commercially pure (99.5 %) titanium sheets (0.2 mm thick) were cut to size, ultrasonically cleaned in alcohol and later chemically polished before being anodized [23]. The chemical polishing solution was composed of HF/ HNO₃/ H₂O in the volume ratio of 1/ 4/ 5. Ti sheets were immersed in polishing solution for a predetermined time (5 s- 40 s) before being immediately taken out and flushed with deionized water.

2.2. Anodization

The pretreated Ti sheets are used as the anode, with a platinum electrode serving as the cathode. The electrolyte consisted of an ethylene glycol based solution containing 2 mass % water and a measured mass % concentration of ammonium fluoride (NH₄F), such as 0.125 % and 0.25 %. Anodization was performed at room temperature by the application of a constant voltage (20–80 V) using a DC power supply (DH1720 A-5); at the same time, the electrolyte was gently stirred. The effect of varying the anodization time from 30 min to 90 min was investigated.

After anodization, the samples were washed in deionized water followed by drying in air, and then annealed at 450 °C for 2 h (in air) using a muffle furnace to enable conversion of the TiO₂ from the amorphous form to anatase; the Ti-based TiO₂ NTs were finally obtained thereafter.

2.3. Morphology and photoelectrochemical characterization

The surface microstructure of chemically polished Ti sheets was observed by an optical metallographic microscope (10XB-PC, Shanghai Optical Instrument Co., Ltd, China). Surface

morphology of TiO₂ NTs was analysed by a field-emission Scanning Electron Microscope (FE-SEM, FEIHelios NanoLab 600i). The photocurrent response of NTs was measured by a potentiostat (Princeton Applied Research PARSTAT 2273) using the NTs as the working electrode, a Pt sheet for the counter electrode and a saturated calomel electrode as the reference electrode, all immersed in a supporting electrolyte of 0.1 M Na₂SO₄. For measurement of the photocurrent density, the working electrode was irradiated by a Xe lamp (CT-XE-450, Sofn Instruments Co., Ltd) with an intensity of 7.7 mW/cm². The Incident Photon to Current Efficiency (IPCE) was calculated by measurement of the spectral response using a Xe lamp and a CT110 monochromator (1/8, Crowntech, Inc. USA) to irradiate the NTs with light of different wavelengths (λ) ranging from 250 nm to 450 nm [24].

After the optimized anodizing conditions to produce the TiO₂ NTs with the maximum photocurrent density and IPCE was got, four samples of TiO₂ NTs (labelled as TiO₂ NTs-1, TiO₂ NTs-2, TiO₂ NTs-3, TiO₂ NTs-4, respectively) grown under the conditions, and the IPCE of the samples were measured.

3. RESULTS AND DISCUSSION

3.1. Effect of polishing time on the Ti sheet surface

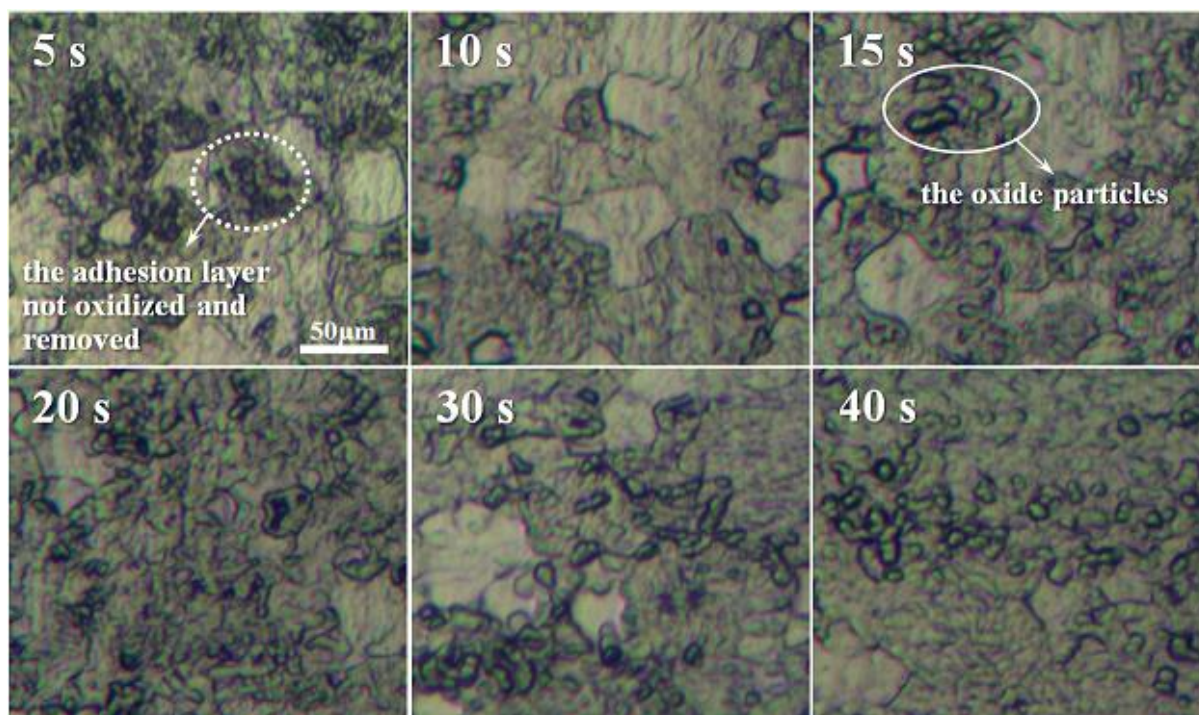


Figure 1. Surfaces of the Ti sheets chemically polished for 5 s- 40 s under a optical metallographic microscope.

Fig. 1 shows micrographs of the surface of Ti sheets taken for varying periods of chemical polishing; the Ti sheet shows changes at the surface with increasing chemical polishing time. After chemical polishing for 5 s, the adhesion layer on the Ti surface was not fully oxidized and removed

(Fig. 1 pointed by the dotted line). For up to 10 s of polishing, the adhesion layer is removed, and the surface of the Ti sheet tends to become more smooth. Next, with further extension of the polishing time, oxide particles begin to accumulate on the surface of the Ti sheet (Fig. 1 pointed by solid line) [25]. Therefore, 10 s of chemical polishing is determined to be optimal for the Ti sheets to have a smooth surface suitable for the growth of the NTs.

3.2. Effect of anodization parameters on the surface morphology of TiO₂ NTs

3.2.1. Anodizing voltage

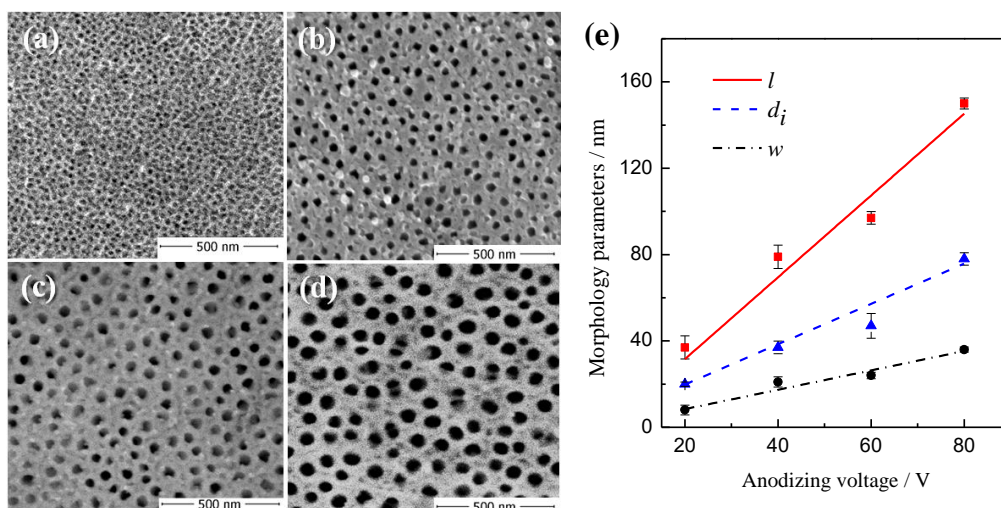


Figure 2. FE-SEM images of the TiO₂ NTs grown at (a), 20 V; (b), 40 V; (c), 60 V; (d), 80 V for 60 min in 0.125 % NH₄F electrolyte. (e), Quasi-linear dependence of the morphology parameters (l , d_i and w) of the NTs on the anodization voltage.

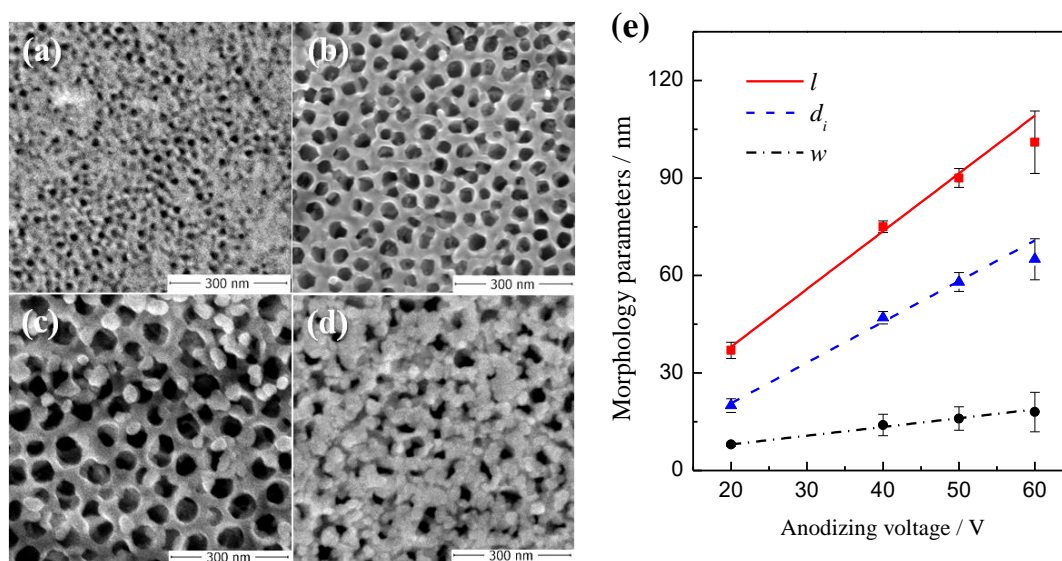


Figure 3. FE-SEM images of the TiO₂ NTs grown at (a), 20 V; (b), 40 V; (c), 50 V; (d), 60 V for 60 min in 0.25 % NH₄F electrolyte. (e), Quasi-linear dependence of the morphology parameters (l , d_i and w) of the NTs on the anodization voltage.

Fig. 2 and Fig. 3 show FE-SEM images of the TiO₂ NTs grown at 20-80 V and the relationship between the anodizing voltage and the morphology of the NTs, as characterized by the main parameters of internal diameter (d_i), centre to centre distance (l) and wall thickness (w), respectively. A quasi-linear relationship is observed between d_i , l and w and the voltage, as shown in Fig. 2 e) and Fig. 3 e). These data are consistent with results obtained in previous studies [7, 10, 26].

Fig. 2 d) and Fig. 3 c) shows particles attached to the surface of the TiO₂ NTs, while Fig. 3 d) shows a flocculent structure (nanosponges) [8]. If the anodizing voltage is too high, the surface of the NTs can dissolve leading to the formation of particles or a sponge-like structure and the destruction of the ordering of the arrays of NTs [11, 27].

The l values for different samples of NTs grown at 60 V were determined to be 109 nm, 97 nm, 95 nm, 105 nm, 98 nm and 97 nm, which are all highly similar to each other, as shown in Fig. 4. These data indicate that l strongly depends on the anodizing voltage and that the use of the same voltage tends to produce NTs with the same l values for the given experimental conditions.

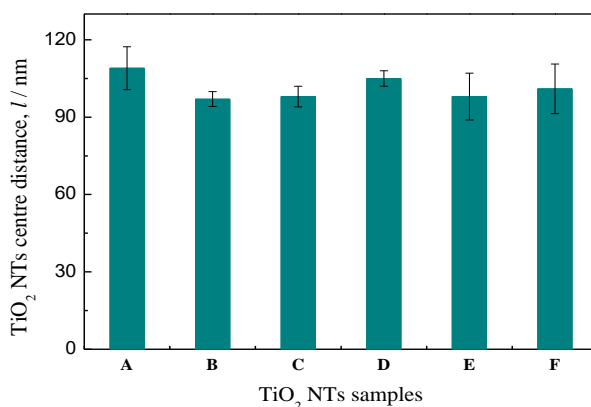


Figure 4. The l values of six samples of TiO₂ NTs grown at 60 V in 0.125 % NH₄F electrolyte for A, 30 min; B, 60 min; C, 90 min; and in 0.25 % NH₄F electrolyte for D, 40 min; E, 50 min; F, 60 min.

3.2.2. Anodizing time

Fig. 5 and Fig. 6 show SEM images of the TiO₂ NTs grown at 60 V for 30 min- 90 min. Fig. 5d shows that as the anodizing time increases from 30 min to 90 min, d_i increases and w decreases, while l is approximately 100 nm for all NTs, which is consistent with the voltage dependence described above. As shown in Fig. 5 c) and Fig. 6 a), nano-particles can also be observed on the surface of the NTs. These nanoparticles are formed and detached from the body of the NTs and, as shown in Fig. 6 b), can become separate particles that assemble to form a nanosponge layer, as shown in Fig. 6 c). The data show that the surface of the NTs can also dissolve with increasing anodization time, and indicate that the formation of ordered nanotube arrays is also dependent on the length of the oxidation time [20].

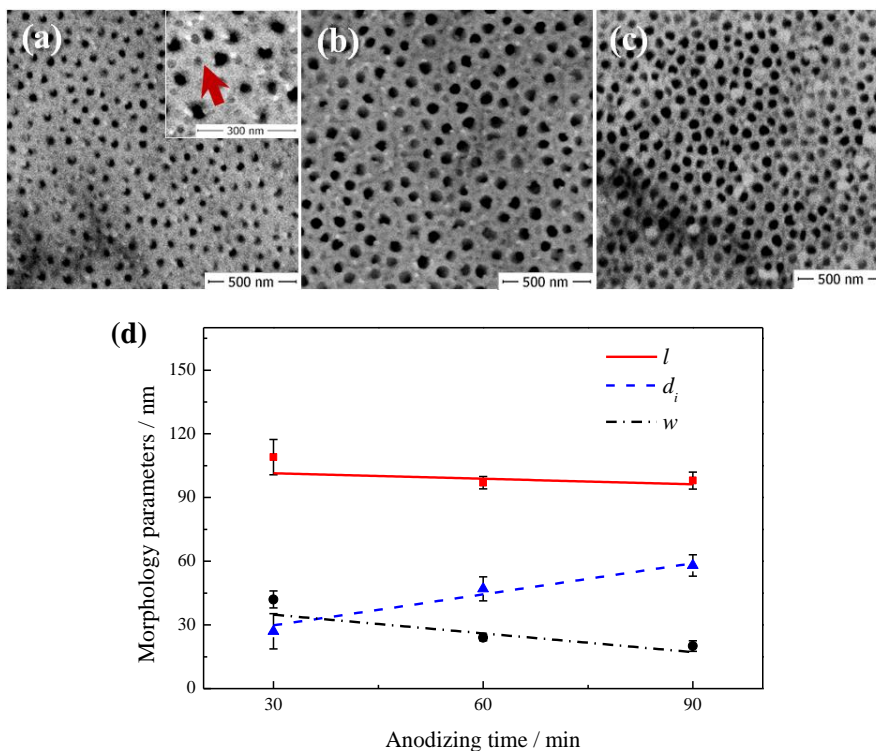


Figure 5. FE-SEM images of the TiO₂ NTs grown at 60 V, for (a), 30 min; (b), 60 min; (c), 90 min in 0.125 % NH₄F electrolyte; (d), Quasi-linear dependence of the morphology parameters (l , d_i and w) of the NTs on the anodizing time.

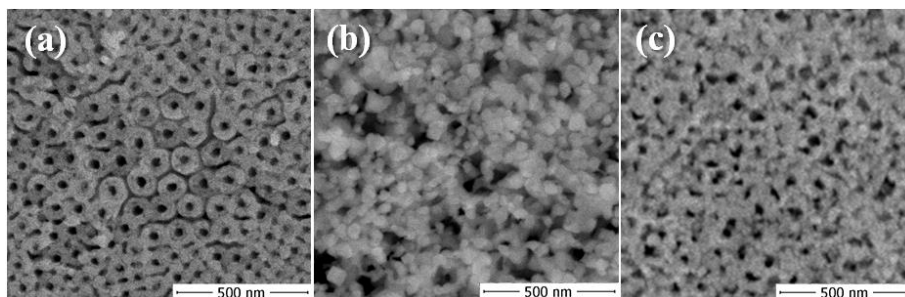


Figure 6. FE-SEM images of the TiO₂ NTs grown at 60 V, for (a), 40 min; (b), 50 min; (c), 60 min in 0.25 % NH₄F electrolyte.

From a closer inspection of the surface, round shallow pits are observed for TiO₂ NTs with thick walls, as noted by the arrow in Fig. 5 a); similar features are also observed in Fig. 2 b). The shallow pits are a signature of the original growth stage of the NTs [8], which are called pore embryos [16] (see below). Therefore, we can determine three stages in the growth process of the NTs. First, the NTs begin to appear and their numbers increase gradually, as shown in Fig. 5 a) and Fig. 2 b); this growth lasts up to the smallest value measured for the distance between centres and depends on the anodizing voltage. Next, NTs form integrated tube arrays, as shown in Fig. 2 a), Fig. 3 b) and Fig. 5 b). In the last stage, the surface of the NTs begins to dissolve, resulting in the formation of nanoparticle and nanosponge morphologies.

3.2.3. NH_4F concentration

By comparing TiO_2 NTs grown in 0.125 % and 0.25 % NH_4F electrolyte, we determine that d_i is smaller in the former electrolyte compared to the latter; in contrast, w is larger in the former compared to the latter, Fig. 2 a), b), c) and Fig. 3 a), b), d). The data indicate that the inner diameter and wall thickness of the NTs depends on the concentration of the NH_4F electrolyte.

3.3. Effect of anodization parameters on the photoelectrochemical properties of the NTs

The photoelectrochemical properties of TiO_2 NTs grown under different anodizing conditions were studied. Fig. 7 shows the photocurrent response measured for NTs used as the working electrode in a photoelectrochemical cell.

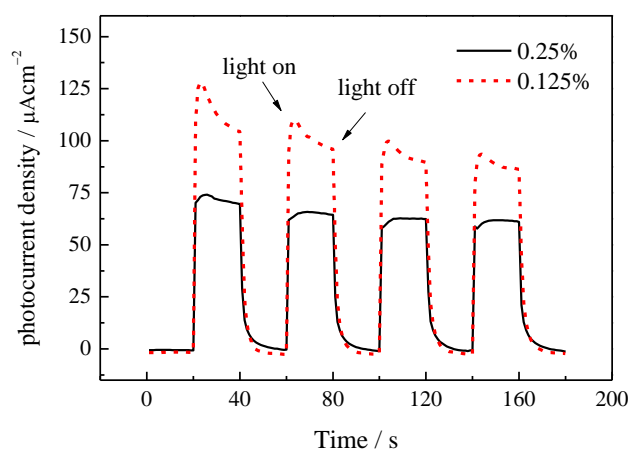
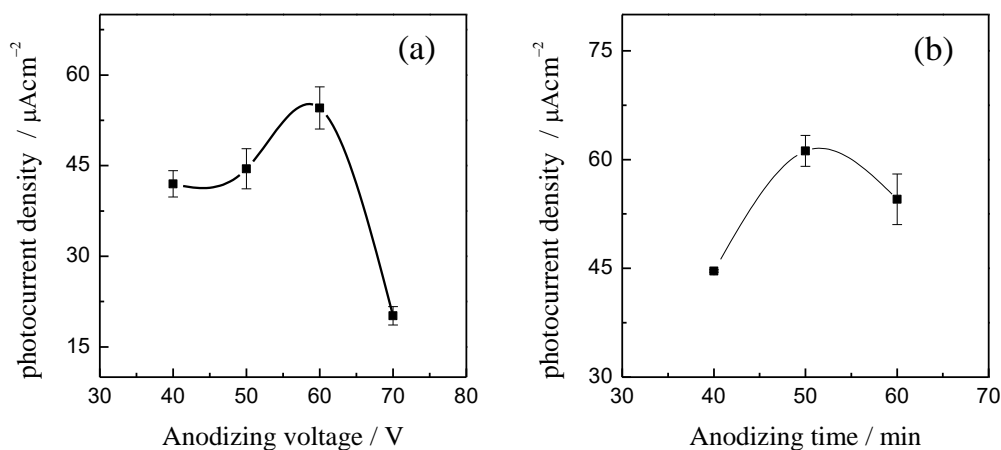


Figure 7. Photocurrent response of TiO_2 NTs grown at 60 V for 60 min in 0.25 % NH_4F electrolyte (solid line) and in 0.125 % NH_4F electrolyte (dotted line).

From the photocurrent response data, the average steady-state photocurrent density (J_p) was calculated and used to compare the photoelectrochemical properties of the TiO_2 NTs.



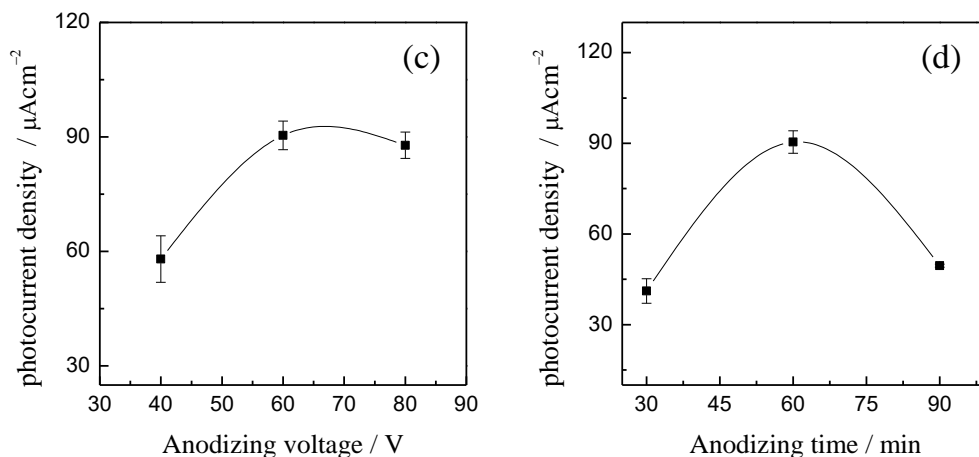


Figure 8. The average photocurrent density (J_p) of TiO_2 NTs grown under different conditions: (a), 40-70 V, 60 min and 0.25 % NH_4F electrolyte; (b), 60 V, 40- 60 min and 0.25 % NH_4F electrolyte; (c), 40- 80 V, 60 min and 0.125 % NH_4F electrolyte; (d), 60 V, 30- 90 min and 0.125 % NH_4F electrolyte.

The dependence of J_p on the anodizing voltage and time and the NH_4F electrolyte concentration is shown in Fig. 8. In the electrolyte with 0.25 % NH_4F , the NTs grown at 60 V for 50 min show a maximum value for J_p of $61.20 \mu\text{A}/\text{cm}^2$; in the electrolyte with 0.125 % NH_4F , NTs grown at 60 V for 60 min show a maximum J_p of $90.42 \mu\text{A}/\text{cm}^2$. Therefore, the optimized combination of anodization parameters can be considered to be an anodizing voltage of 60 V, anodizing time of 60 min and 0.125 % NH_4F electrolyte concentration for the given experimental conditions.

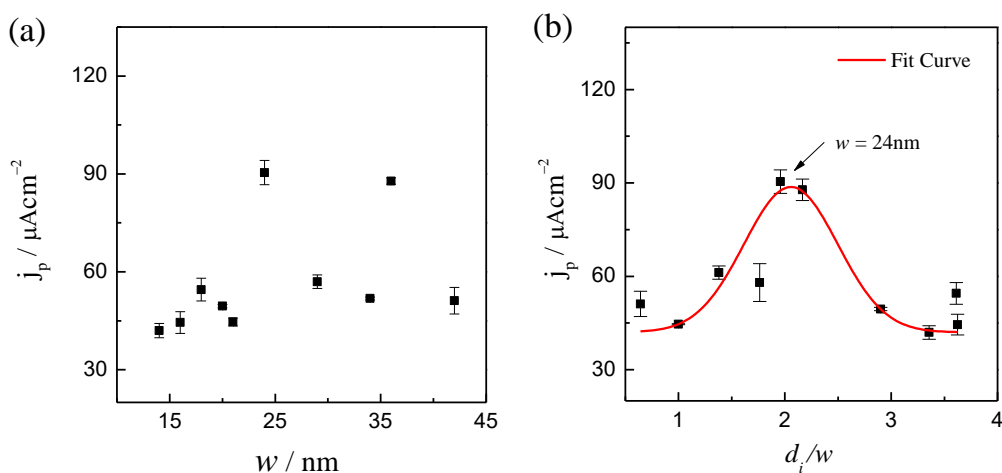


Figure 9. The relationship between (a) the photocurrent density (J_p) and wall thickness (w), (b) the photocurrent density (J_p) and the ratio of the diameter to the wall thickness (d_i/w) of TiO_2 NTs shown in Fig. 8.

Fig. 9 a) shows the dependence of J_p on the wall thickness of the TiO_2 NTs. For $w < 24 \text{ nm}$, the data for all the samples show a relatively small photocurrent (also shown in Fig. 8); for $w > 24 \text{ nm}$, the photocurrent shows no obvious correspondence with the wall thickness. Fig. 9 b) shows the measured photocurrent versus the ratio of the diameter of the NTs to the wall thickness (d_i/w) and a curve fit to

the data. It can be clearly seen from the curve fit that for a d_i / w of 2, the NTs show the highest photocurrent value. A wall thickness for the NTs that is either too large or too small compared to the diameter will lead to a decrease in the photocurrent.

Fig. 10 shows the IPCE spectra of four samples of TiO_2 NTs all grown under the same optimized anodizing conditions, as detailed above. It is clear that the four samples show substantially uniform IPCE spectra, with a peak at 300 nm corresponding to a maximum IPCE of $17.8 \pm 1.0 \%$. This finding indicates that the use of the optimized conditions for anodization can result in a photoelectrochemical response of the NTs that shows good reproducibility.

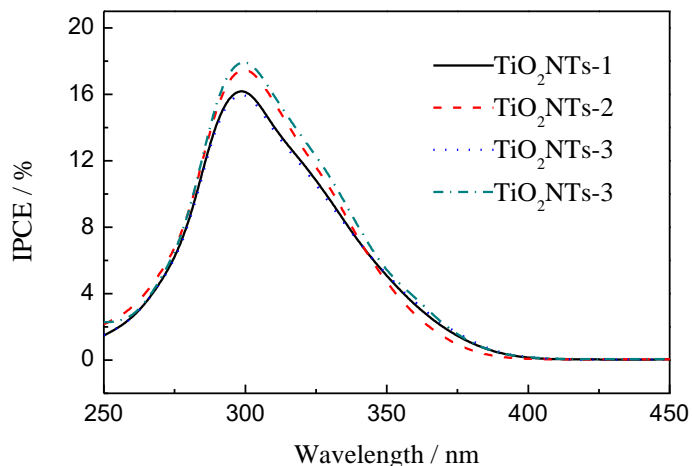


Figure 10. IPCE spectra of TiO_2 NTs grown under the same anodizing conditions, i.e., 60 V, 60 min and 0.125 % NH_4F electrolyte.

3.4. Discussion

3.4.1. Effect of anodization parameters on the surface morphology of the TiO_2 NTs

Formation mechanisms for the TiO_2 NTs have been reported in recent years [14-17, 28]; the combination of a theory of avalanche breakdown [15], viscous flow model [14] and oxygen bubble model [16] can be used to explain the effect of anodization parameters on the surface morphology of NTs. In the early stage of anodic oxidation, there are two currents flowing in the oxide film on the Ti surface; an ion current (j_{ion}) and an electron current (j_0). As the oxide film gradually thickens, j_{ion} decreases, and j_0 increases [28]. Once a critical thickness is reached, the oxide film undergoes avalanche breakdown (with an avalanche electron current j_e) and generates oxygen [15, 17]. Oxygen first aggregates into bubbles in the oxide film and later bursts through the surface of the oxide film to form pore embryos (noted by the arrow in Fig. 5 a)). The oxide film gives rise to viscous flow around the outside of the bubble, which results in the growth of holes that eventually form an NT structure [16].

Fig. 2 and Fig. 3 show a quasi-linear relationship between l and the anodization voltage, and Fig. 4 shows that at the same voltage, TiO_2 NTs with the same l can be obtained. From the theoretical models discussed above, it can be suggested that the oxygen bubbles are generated at different

positions in the pollution layer until the bubble spacing is smaller than the bubble diameter. Therefore, the centre to centre distance, l , of the NTs depends on the diameter of the oxygen bubbles, d_{O_2} , i.e., $d_{O_2} < l < 2 d_{O_2}$. The oxygen bubble diameter is controlled by the amount of oxygen generated in the oxide film before bursting. Since the oxygen is generated by the electron current after avalanche breakdown, with the avalanche electronic current being proportional to the oxidation voltage [15, 16], it can be inferred that increasing oxidation voltage increases the oxygen bubble diameter, which subsequently leads to a proportional increase in the distance between centres of the TiO₂ NTs.

As the oxidation time increases, the wall thickness, w , decreases or large floccules are produced on the surface of the NTs, as shown in Fig. 5 and Fig. 6; this is due to the dissolution of F⁺ in the electrolyte. In the NT formation process, w depends on the thickness of the oxide film [16]; at the same time, the presence of F⁺ will lead to the dissolution of NTs at the surface [20]. Therefore, the walls of the NTs become thinner, and floccules can even form on the surface of the NT array, when the dissolution becomes stronger. For longer oxidation times and increased F⁺ concentration, the dissolution becomes more clear.

3.4.2. Effect of anodization parameters on the photoelectrochemical properties of the TiO₂ NTs

Anodization parameters can influence the photocurrent response of TiO₂ NTs by changing the microstructure of the material such as the wall thickness and the ratio of the diameter to the wall thickness, d_i / w . Sun et al. [18] reported a critical value for w of NTs, which, if exceeded, leads to the development of a space charge layer and bending of the conduction band edge upwards in the NT surface layer adjacent to the electrolyte; this creates a potential barrier for injected photoelectrons transferring into the redox couples in the electrolyte. As a result, more photoelectrons move towards the electrode in the wall resulting in a higher photocurrent density. The width of the space charge layer is approximately 12 nm for the anatase structure [18,19]. Once w reaches twice the layer width (24 nm), potential barriers form on both sides of the wall, which significantly increases the photocurrent [19]. As shown in Fig. 9 a), NT electrodes with w less than 24 nm, show relatively low values for j_p , while electrodes with $w = 24$ nm show the maximum j_p value. This result is consistent with the theory discussed above. On the other hand, increasing w with respect to the diameter also reduces the roughness of the electrode surface, which will affect the contact area between the electrode and the electrolyte [19], finally leading to a reduction in the rate of electrons injected into the NTs. The observed correspondence between the d_i / w and the measured photocurrent response of the TiO₂ NT electrodes shown in Fig. 9 b) is a comprehensive reflection of the two cases discussed above. For $w < 24$ nm and $d_i / w > 2$, NT electrodes show high degrees of surface roughness; however, sufficient barriers cannot form under these situations, therefore the photocurrent will be small (on the right side of the fitting curve). Although sufficient barriers can form in NTs electrodes with $w > 24$ nm and $d_i / w < 2$, the degree of roughness is small, and the photocurrent values are also small (on the left side of the fitting curve). The photocurrent values for either of these two types of NT electrodes is smaller than that of NT electrodes with $w \approx 24$ nm and $d_i / w \approx 2$.

4. CONCLUSIONS

We studied the effect of anodization factors on the surface morphology and the photoelectrochemical properties of TiO₂ NTs. The following conclusions are drawn from this work. The anodizing voltage can influence the distance between NT centres, while the anodizing time and NH₄F electrolyte concentration can affect the inner diameter and wall thickness. Any one of these three factors, if too large, can destroy the orderliness of the NT array surface. Changing the anodization parameters can also change the photocurrent response of the NTs by affecting the microstructure of the material, such as the wall thickness. The optimized combination of anodization parameters is determined to be an applied voltage of 60 V, anodizing time of 60 min and 0.25 % NH₄F electrolyte under given experimental conditions. These anodization conditions were used to fabricate TiO₂ NTs with a wall thickness of approximately 24 nm that demonstrated relatively high photocurrents. Grown under optimized conditions, TiO₂ NTs showed a maximum photocurrent density of 90.42 $\mu\text{A}/\text{cm}^2$ and peak IPCE of $17.7 \pm 1.0\%$ with good reproducibility.

ACKNOWLEDGMENT

The authors wish to acknowledge the supports of the “Fundamental Research Funds for the Central Universities” and “Natural Science Foundation of Hebei Province 2016”.

References

1. B. O'regan, M. Gratzel, *Nature*, 353 (1991) 737.
2. M. K. Nazeerudin, A. Kay, I. Rodicio, R. Humphry-Baker, E. Mueller, N. Vlachopoulos and M. Gratzel, *J. Am. Chem. Soc.*, 115 (1993) 6382.
3. Z. Zhang, C. C. Wang, R. Zakaria and J. Y. Ying, *J. Phys. Chem. B.*, 102 (1998) 10871.
4. M. Paulose, O. K. Varghese, G. K. Mor, C. A. Grimes and K. G. Ong, *Nanotechnology*, 17 (2006) 398.
5. Q. W. Chen, D. S. Xu, *J. Phys. Chem. C.*, 113 (2009) 6310.
6. J. Park, S. Bauer, K. Mark and P. Schmuki, *Nano Lett.*, 7 (2007) 1686.
7. Próspero Acevedo-Peña, Ignacio González, *Procedia Chem.*, 12 (2014) 34.
8. K. Lee, A. Mazare, P. Schmuki, *Chem. Rev.*, 114 (2014) 9385.
9. K. Lee, P. Schmuki, *Electrochimica Acta*, 100 (2013) 229.
10. D. Regonini, A. Satka, A. Jaroenworuluck, D.W.E. Allsopp, C.R. Bowen and R. Stevens, *Electrochimica Acta*, 74 (2012) 244.
11. B. Munirathinam, H. Pydimukkala, N. Ramaswamy and L. Neelakantan, *Appl. Surf. Sci.*, 355 (2015) 1245.
12. D. Regonini, C.R. Bowen, A. Jaroenworuluck and R. Stevens, *Mat. Sci. Eng. R.*, 74 (2013) 377.
13. K.M. Deen, A. Farooq, M.A. Raza and W. Haide, *Electrochimica Acta*, 117 (2014) 329.
14. S.J. Garcia-Vergara, P. Skeldon, G.E. Thompson and H. Habazaki, *Electrochimica Acta.*, 52 (2006) 681.
15. J. M. Albella, I. Montero, J. M. Martinez-Duart, *Electrochim. Acta.*, 32 (1987) 255.
16. S. Zhang, D. Yu, D. Li, Y. Song and J. Che, S. You and X. Zhu, *J. Electrochem. Soc.*, 161 (2015) E135.
17. A.C. Crossland, H. Habazaki, K. Shimizu, P. Skeldon, G.E. Thompson, G.C. Wood, X. Zhou and C.J.E. Smith, *Corros. Sci.*, 41 (1999) 1945.
18. L. Sun, S. Zhang, X. Sun and X. He, *J. Nanosci. Nanotechnol.*, 10 (2010) 4551.

19. X. Gao, J. Chen, C. Yuan, *J. Power Sources*, 240 (2013) 503.
20. D. Regonini, F.J. Clemens, *Mater. Lett.*, 142 (2015) 97.
21. I. Paramasivam, H. Jha, N. Liu and P. Schmuki, *Small*, 20 (2012) 3073.
22. J. Augustynski, B. Alexander, R. Solarska, *Top. Curr. Chem.*, 303 (2011) 1.
23. S. Zhang, K. Liang, Y. Tan, *Acta Phys. -Chim. Sin.*, 27 (2011) 2726.
24. Y. Tan, S. Zhang, K. Liang, *Nanoscale Res. Lett.*, 9 (2014) 67.
25. X. Zhang, X. Luo, J. Zhang, *Chin. J. Dental Mater. Device*, 14 (2005) 69.
26. A. Valota, M. Curioni, D.J. Leclere, P. Skeldon, P. Falaras and G.E. Thompson, *J. Electrochem. Soc.*, 157 (2010) K243.
27. H. Li, R. Chen, C. Ma, S. Zhang, Z. An and W. Huang, *Acta Phys. -Chim. Sin.*, 27 (2011) 1017.
28. J. Wang, H. Fan, H. Zhang, Q. Chen, Y. Liu and W. Ma. *Prog. Chem.*, 28 (2016) 284.

© 2017 The Authors. Published by ESG (www.electrochemsci.org). This article is an open access article distributed under the terms and conditions of the Creative Commons Attribution license (<http://creativecommons.org/licenses/by/4.0/>).